Wideband Inter-Beam Interference Cancellation for mmW/Sub-THz Phased Arrays With Squint

Muhammad Yasir Javed, *Graduate Student Member, IEEE*, Nuutti Tervo, *Member, IEEE*, Marko E. Leinonen, *Member, IEEE*, and Aarno Pärssinen, *Senior Member, IEEE*

***Abstract*—As relative bandwidth increases, beam squint, i.e., frequency dependent directivity, limits the wideband performance of phase-shifter steered arrays. This effect is already notable in 5G systems operating at 28 GHz and above with 400/800 MHz bandwidths, especially if broadband cancellation is needed between multiple beams. The wideband squinting effect reduces the signal-to-interference-plus-noise-ratio of a multibeam system by changing the level and direction of the spatial null towards the interferer. This paper examines the effectiveness of the inter-beam interference (IBI) cancellation using crosscoupled signals for wideband arrays with visible squint effect. For a large relative bandwidth of the array, this paper presents a component carrier-based approach for interference cancellation between the beams of different users or data streams. Furthermore, as bandwidth and array size increase, the impact of squint increases, which is also examined for the cancellation of the IBI. Furthermore, an example scenario is simulated using standard 5GNR modulated waveforms.**

***Index Terms*—Beam synthesis, carrier aggregation, interference nulling, millimetre wave communication, squinting effect, ultra wideband communication, wideband spatial effect.**

I. Introduction

MILLIMETER-WAVE (mmW) and Sub-terahertz (Sub-THz) communication having bandwidths on the order of gigahertz (GHz) or tens of GHz, are seen as promising technologies for the 5G and 6G wireless systems [1], [2], [3], [4]. Communication in these bands will alleviate the spectrum scarcity and capacity limitations of current wireless systems. However, these frequencies suffer from significant path and propagation losses per antenna element, posing a serious challenge to practical communications [5], [6]. The wavelengths of the frequencies in these bands, on the other hand, are shorter allowing more antennas to be packed into the same physical space. For mmW and Sub-THz communications, this results in the implementation of large-scale antenna arrays with spatial multiplexing capabilities and highly directional beamforming gains [7]. Link range analysis for 5G [8] and 6G [9] systems give insights to these challenges.

Traditional fully digital beamforming systems are not practical for mmW/Sub-THz frequencies. This is because they require one dedicated radio frequency (RF) transceiver chain per antenna element, which is not cost and power efficient to implement in case of very large arrays and bandwidths. Analog beamforming, on the other hand, can have only one baseband chain and enabling only single-stream transmission [10]. Hybrid digital/analog beamforming systems offer a compromise on the performance/complexity trade-off [11], [12]. In hybrid digital/analog radio systems, the beamforming process is split between digital and analog domains. The digital domain beamforming is used to spatially multiplex users or separate data streams and the analog domain beamforming is used to improve the effective-isotropic-radiated power (EIRP) and thus range. Beam power differences even for a single MIMO link might be large [13] and require directive cancellation to avoid co-channel interference due to inter-beam effects.

To achieve full array gain in hybrid beamforming designs, analog RF beamformers produce directional beams aligned with the physical directions of the propagation channels of the users [14]. Furthermore, the phase control of the array antenna elements enables beam scanning capability [15]. A phase shifter is typically utilized in each antenna of the array to steer the beam in space with reasonable cost and ease of implementation [16], [17] as shown in Fig. 1. Additionally, the phase shifter for each antenna can be calibrated for the carrier frequency of the system [18]. Such phase shifter based analog RF beamformers work well for small relative bandwidths. However, when frequency-dependent phase shifters are used for the wideband, the beams of different frequencies point in slightly different spatial directions. This leads to wideband spatial effect, known as beam squint in the frequency domain [19], [20], [21]. In a multi-user multi-beam system, the main lobes of the beams are directed towards the intended users for maximizing the power, while the nulls are formed towards the potential victims of the interference, for example, other users [22]. Squinting reduces spatial selectivity in wideband transmission, resulting in a reduction in null depth towards the other beams and so decreasing their SINRs.

Wideband interference between the beams can be eliminated by placing multiple adjacent nulls in the radiation pattern [23], [24]. Wide nulls in specified directions can also be generated by constraining the adaptive weights when synthesizing an antenna

Manuscript received 5 July 2022; revised 8 November 2022; accepted 7 January 2023. Date of publication 3 February 2023; date of current version 20 June 2023. This work was supported in part by Nokia Corporation Ltd., in part by the RF Sampo under Project 3071/31/2021, in part by the Academy of Finland 6Genesis Flagship under Grant 346208, and in part by the Business Finland Project 5G-FORCE. The review of this article was coordinated by Prof. Yue Gao. *(Corresponding author: Muhammad Yasir Javed.)*

The authors are with the Centre for Wireless Communications - Radio Technologies, University of Oulu, FI-90014 Oulu, Finland (e-mail: yasir.javed@oulu.fi; nuutti.tervo@oulu.fi; marko.e.leinonen@oulu.fi; Aarno.Parssinen@oulu.fi).

Digital Object Identifier 10.1109/TVT.2023.3242133

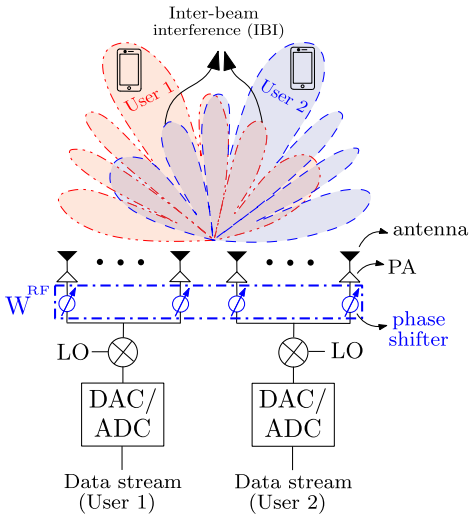

Fig. 1. Inter-beam interference (IBI) in hybrid multibeam phased array architecture.

pattern stochastically [25], [26], [27]. It is sometimes more convenient to design an array with decreased sidelobe levels to all directions rather than an adaptive wide null in the direction of the interfering signal. However, null formation and sidelobe suppression in these techniques require full control of all excitation coefficients, which can take the form of amplitude-and-phase control, phase-only control, or amplitude-only control of the array elements. However, the amplitude control deteriorates the power amplifier (PA) efficiency and limits the achievable EIRP in the transmitter. For an RF transmitter, this is challenging because if the amplitude of each RF branch is controlled for interference reduction, the parallel antenna-specific PAs experiences different shapes of nonlinearity which makes the array linearization challenging [28], [29]. In the receiver, amplitude control over the array elements also affects to the overall noise figure [30]. Full control in mmW/Sub-THz phased arrays becomes prohibitively expensive and the system becomes complex as the number of array elements increases.

Another technique used in [31] divides the transmit signal into independent subbands using a filter bank behind each array element and then uses a tapped delay line (TDL) in each subband to generate frequency invariant spatial nulls in the radiation pattern of the array. However, the design of highly linear and sharp filters is highly complicated, and their implementation is restricted due to their larger power consumption and limited operating frequency range [32]. Multiple arrays can be used to create nulls in specific spatial directions in subarray-based systems [33], [34]. Using the additional array solely for the purpose of creating nulls, on the other hand, is a waste of antenna area. While each subarray can create beams for specific users, it can also be used to cancel interference without affecting the amplitude or phase excitation within the subarray. In fact, such a method can use RF beamformers to create the desired nulls. The two-stage beamforming technique analyzed in this paper uses cross-connected signal paths before splitting to multiple antennas to cancel interference and RF beamformers to improve beam EIRP. In this paper, interference cancellation in wideband arrays with squint is described using a component carrier-based approach. Additionally, when bandwidth and array size increase, the impact of squint increases, which is also examined for the cancellation of the IBI. Furthermore, an example scenario is recreated utilizing standard 5GNR modulated waveforms. This is specifically suitable for the waveforms used for example in 5GNR [35]. The rest of the article is organized as follows. Section II explains the interference cancellation technique for the narrowband and wideband signals. The simulation analysis is reported in Section III. Finally, the conclusions are given in Section IV.

Notation: Lower-case and upper-case boldface letters denote vectors and matrices, respectively; $(\cdot)^T$, $(\cdot)^H$, and $(\cdot)^{-1}$ denote transpose, conjugate transpose and inverse of a matrix, respectively.

II. Inter-Beam Interference Cancellation in Multi-Beam Systems

We consider a multi-user multi-antenna hybrid beamforming system model in which uniform linear subarrays (ULSAs) are stacked on top of each other at the base station (BS) to generate spatially directed beams. Although not necessarily optimal for practical implementation, this gives clear interrelation for observations assuming that the radio devices are located roughly in the same elevation angle. In the three dimensional (3D) coordinate system, x>0 is the direction of propagation (normal of the array). The azimuth angle ϕ is defined as the angle from positive x-axis towards to y-axis, and the elevation angle θ is the angle from positive x-axis towards the z-axis. Antenna array panel is a two-dimensional rectangular array with M rows and N columns. Each row is a ULSA and connected with a separate RF chain to serve a distinct user in space. In total, for M rows, there are M RF chains serving the M users. The channel between BS and all the M single antenna users is a matrix ($\mathbf{H} = [\mathbf{h_1}, \mathbf{h_2}, \ldots, \mathbf{h_M}]^T \in \mathbb{C}^{M\times N}$). The m^{th} row of the $\mathbf{H}$ represents the line-of-sight (LOS) channel from the user m to BS and given as

$$\mathbf{h}_m = [1, e^{jkr_{m,2}}, \ldots, e^{jkr_{m,N}}], \tag{1}$$

where $\mathbf{k}$ is the wave vector and describes the phase variation of a plane wave in three orthogonal directions as a function of position and frequency, expressed as $k = 2\pi f/c(\cos\theta\cos\phi, \cos\theta\sin\phi, \sin\theta)$, where f is the operating frequency, and c is speed of light in free space. $\mathbf{r_{m,n}}$ represents position for the nth antenna of the mth row on the antenna panel. We employ maximum ratio transmit (MRT) beamforming to achieve maximum EIRP for the RF analogue beamformers, which is the conjugate transpose of the channel matrix, given as

$$\mathbf{W}_{RF} = \mathbf{H}^H, \tag{2}$$

where $\mathbf{W}_{RF} \in \mathbb{C}^{N\times M}$. The RF beamformers implemented with phase shifters are modelled to correspond various time delays for distinct carrier frequencies, causing the radiation pattern to squint as a function of frequency. In other words, effective channel ($\mathbf{H}_e$) is the channel that beamformers encounter at a

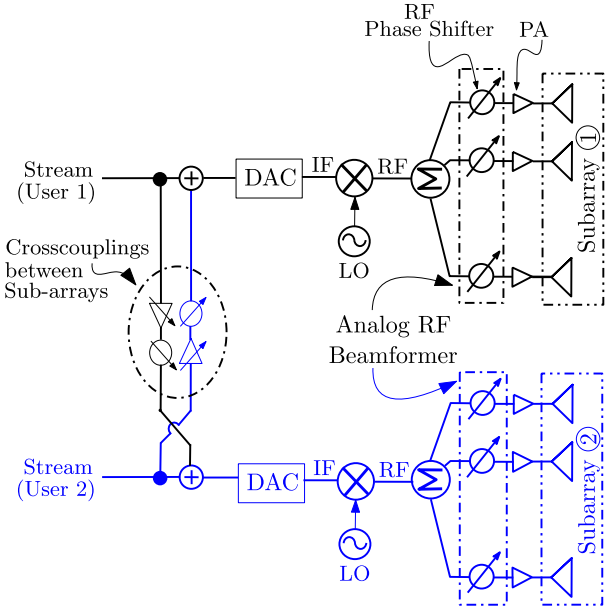

Fig. 2. Subarray based hybrid beamforming architecture.

particular frequency and hence the effective channel changes over the entire signal band. Effective channel for a frequency f is mathematically expressed as

$$\mathbf{H}_e^f = \mathbf{H}^f \mathbf{W}_{RF}, \tag{3}$$

where $\mathbf{H}^f$ is the channel seen at frequency f between the BS and the users. The $\mathbf{H}_e^f$ is a square matrix of the order of M with diagonal entries representing powers of the beams toward users and non-diagonal elements representing interference between users. The information from the effective channel in (3) can be used to compute the SINR over the bandwidth ($B = f_2 - f_1$). The SINR (γ) of the m^{th} user with MRT analog beamformer is given as

$$\boldsymbol{\gamma}_m^{MRT} = \frac{\int_{f_1}^{f_2} |(\mathbf{H}_e^f)_{m,m}|^2 df}{\sum_{i \neq m}^{N_u} (\int_{f_1}^{f_2} |(\mathbf{H}_e^f)_{m,i}|^2 df) + \sigma_m^2}, \tag{4}$$

where σ_m^2 is the noise variance with zero mean for channel to the user m and N_u is the total number of users.

A. Narrowband IBI Cancellation (NB-IBIC)

The subarray of a user can be used to steer beam in the direction of the desired base station for radio signals, and the same subarray can also be utilized to produce the required notches to cancel interference from other subarrays. Therefore, each subarray can be crosscoupled (connected) to the other in the baseband (BB), intermediate frequency (IF), or radio frequency (RF) to eliminate mutual interference between them as shown in Fig. 2. The crosscoupled signals from the crosscouplings between the subarrays are phase-inverted (opposite phase) and scaled down to the degree of interference. Fig. 3 illustrates the beams of the usable signals and the beams of the IBI cancellation or cross-coupled signals. The crosscoupled signals are transmitted over-the-air (OTA) in the directions of the beams, as shown in the Fig. 3 for two users. The crosscoupled signals have the same amplitude as the degree of interference in those directions, but

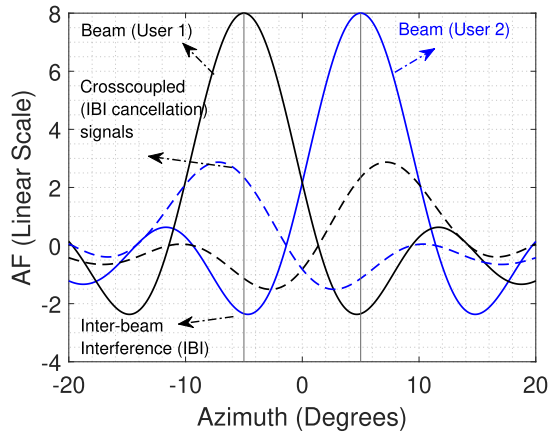

Fig. 3. Illustration of the cancellations of the IBI with the crosscoupled signals.

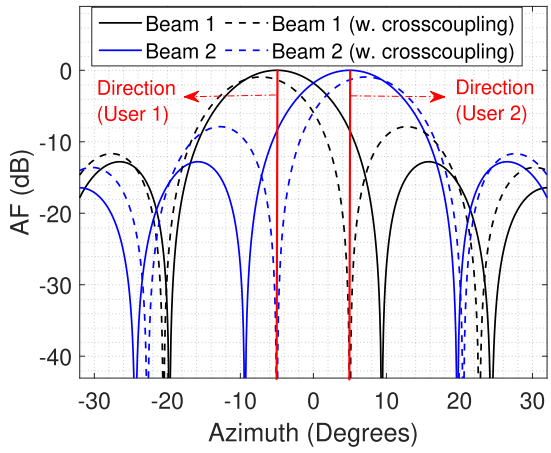

Fig. 4. Spatial response of the two beams with and without inter-beam interference cancellation (IBIC).

their phases are opposite. The interference and crosscoupling signals combine destructively and cancel each other in the appropriate directions. Fig. 3 depicts such an illustration with two beams in linear scale. The cancellation results in a null in beam 2 interference in the direction of beam 1 and vice versa as shown in Fig. 4. The cancellation has a minor effect on the main lobe gain. When the separation between the beams increases, the proposed approach has less of an effect on main lobe gain.

The concept of the effective channel can also be used to define cross-coupling coefficients, given as

$$\mathbf{A}^f = ((\mathbf{H}_e^f)^H \mathbf{H}_e^f)^{-1} (\mathbf{H}_e^f)^H. \tag{5}$$

$\mathbf{A}^f \in \mathbb{C}^{M \times M}$ with non-diagonal elements representing cross-coupling coefficients for the cancellation of the inter-beam interference at frequency f. The SINR (γ) of the m^{th} user with inter-beam interference cancellation (IBIC) by crosscoupling is given as

$$\gamma_m^{IBIC} = \frac{\int_{f_1}^{f_2} |(\mathbf{H}_e^f)_{m,m}|^2 df}{\sum_{i \neq m}^{N_u} (\int_{f_1}^{f_2} |(\mathbf{H}_e^f \mathbf{A}^f)_{m,i}|^2 df) + \sigma_m^2}. \tag{6}$$

Crosscouplings cancel the IBI, resulting in a deep null in the spectrum of the IBI at the crosscoupling frequency as shown in Fig. 5. Due to squint effects, the cancelling performance

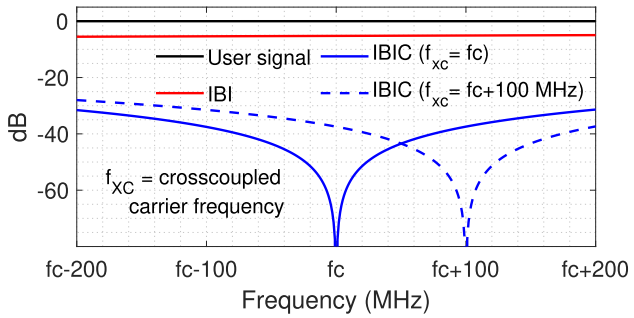

Fig. 5. Spectrums of the user signal, IBI, and cancelled IBI at carrier frequency and cancelled IBI at offset from carrier frequency.

worsens at frequencies that are at offset from the crosscoupling frequency. On the other hand, it can also be seen in Fig. 5 that if the cancellation frequency is altered by changing the phase of the crosscoupled signal while using the same beamformers, the IBI cancellation null in the spectrum changes as well. Therefore, crosscoupling-based IBI cancellation enables IBI cancellation at any frequency in the band without requiring the RF beamformers to be changed. This independence is used for the cancellation of the wideband IBI.

B. Wideband IBI Cancellation (WIBIC)

Carrier aggregation (CA) is a provision of the wideband transmission standards. CA combines multiple component carriers (CCs) to improve spectral efficiency and throughput. This method nicely channelizes signals in frequency domain, and this enables a separate crosscoupling connection for each CC in order to achieve wideband cancellation of the IBI. A CC-based wideband multibeam phased array architecture is shown in Fig. 6. The crosscouplings are implemented in the baseband in this case. However, depending on the ease of implementation in terms of power consumption, size, and cost, IF and RF realizations are also possible [36]. This method employs MRT for analog RF beamformers primarily for the purpose of achieving maximum EIRP. The RF analog beamformers for all the CCs of one user have same power. However, each CC of one user is crosscoupled separately with the corresponding CC of the other user. A common digital-to-analog converter (DAC) is illustrated after the aggregation of the CCs in this example, but it can also be placed before the aggregation separately for each CC depending on the signal generation architecture. Furthermore, with the use of a unitary amplitude distribution for the RF branches, the parallel antenna-specific PAs exhibit comparable nonlinearity shapes, making array linearization less complex. The SINR (γ) of the m^{th} user with inter-beam interference cancellation (IBIC) with multiple crosscouplings is given as

$$\gamma_{cc,m}^{IBIC} = \frac{\sum_{cc}^{N_{cc}} \int_{f_{cc}-\Delta F/2}^{f_{cc}+\Delta F/2} |\left(\mathbf{H}_e^{f_{cc}}\right)_{m,m}|^2 df}{\sum_{i\neq m}^{N_u} \sum_{cc}^{N_{cc}} \left(\int_{f_{cc}-\Delta F/2}^{f_{cc}+\Delta F/2} |\left(\mathbf{A}^{f_{cc}} \mathbf{H}_e^{f_{cc}}\right)_{m,i}|^2 df \right) + \sigma_m^2}, \tag{7}$$

where N_{cc} is number of CCs, f_{cc} is center frequency of each component carrier, ΔF represent the bandwidth of the component carrier, and $\mathbf{A}^{f_{cc}}$ is the matrix of the crosscoupling coefficients calculated at f_{cc}. The SINR with interference cancellation is derived in (6) for the narrowband transmission and (7) for the CC-based wideband transmission in phased arrays. These derivations are given as generic formulas, and their performance is dependent on a variety of parameters. The entire SINR metric is presented as an integral, or channel power, over the intended signal bandwidth in a specific direction. The equations show that a variety of factors, including the array length (number of antenna elements), the scanning angles of the user beam and the interferer, and the relative bandwidth of the array, have an impact on the overall SINR performance.

The wideband IBI in Fig. 7 is cancelled using crosscouplings one and two. In the case of two crosscouplings, the IBI on both sides of the symmetric band is cancelled by a single crosscoupling. The crosscoupling frequency is set at a 100 MHz offset from the carrier frequency on either side of the symmetric band. Each crosscoupling produces a deep null or deep cancellation in the IBI spectrum, which deteriorates as the offset from the crosscoupling frequencies increases. Therefore, the wideband IBI spectrum can be cancelled at various band offsets using multiple crosscoupling. For the specified relative bandwidth of the array, the number of crosscouplings and their offset from the carrier frequency can be determined to satisfy the requirements for IBI cancellation. The cancellation bandwidth is determined by the cancellation requirement as well as the array size. If CC bandwidth is chosen appropriately it is possible to implement CC-based cancellation for a large number of subcarriers. This can relax subcarrier-based processing requirements of fully digital MIMO solutions as anticipated for example in 5G systems.

III. Simulation Analysis

The two beams can interfere with each other via their major lobes (main and side), nulls, or somewhere in between, depending on the angular separation. The wideband squinting effect changes with the relative bandwidth of the array, the scanning angles between the main lobe and the interference, and the number of antennas in the array. It also means that the IBI under squint is affected by the given array parameters, which also means that it has an impact on the cancellation of the IBI as well. Therefore, this simulation section is divided into three subsections. In the first subsection, IBI is examined under the squinting effects. The second subsection examines the influence of squinting on the cancellation of the wideband IBI, while the third subsection examines IBI and cancellation with standard 5GNR modulated waveforms.

A. Wideband IBI Under Squint

A two-beam scenario is simulated using a 32-element ULSA for each beam stacked on top of each other. The spacing between antennas in rows and between rows are fixed to half the wavelength of the carrier frequency. In the simulation analysis, we make use of the relative bandwidth ($RBW = B/f_c \cdot 100\%$), which is always relative to the given carrier frequency. For

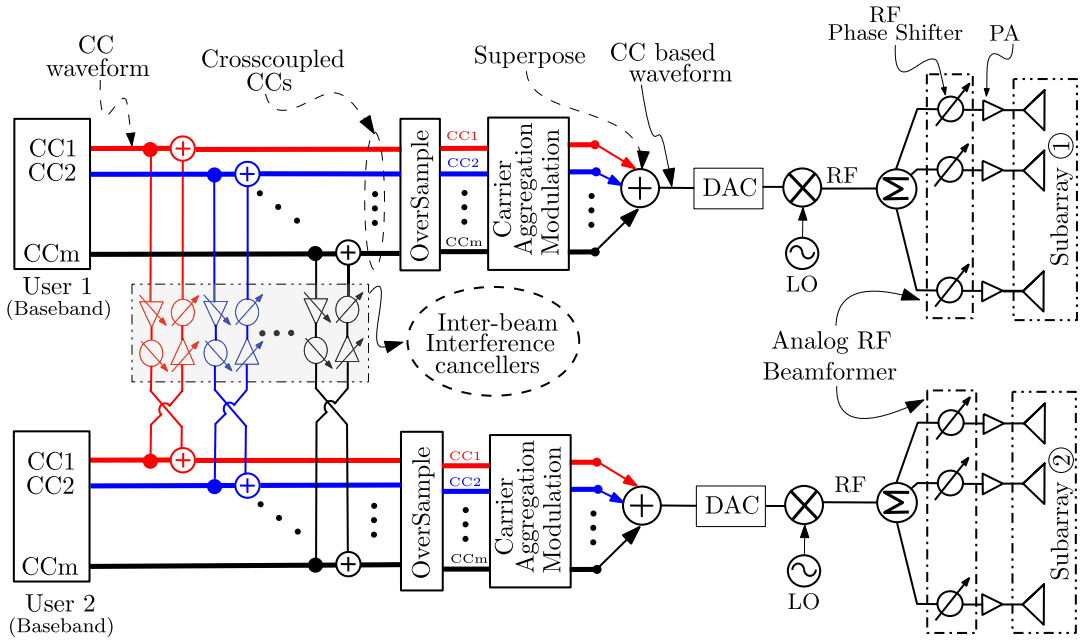

Fig. 6. Component carrier (CC) based wideband multibeam phased array architecture.

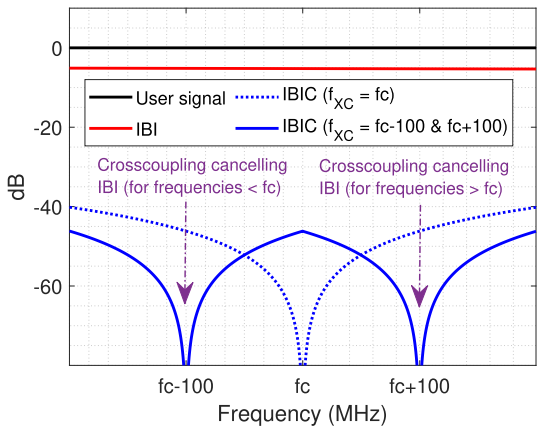

Fig. 7. Impact of IBI with one and two crosscouplings at carrier frequency of 28 GHz.

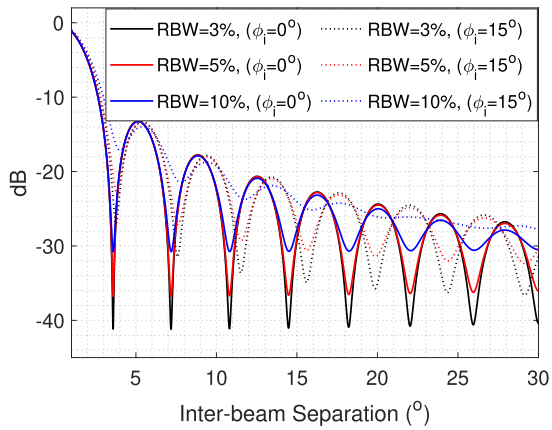

Fig. 8. Squinting impact on the wideband IBI at various inter-beam separations.

instance, the RBW of 10% at 30 GHz carrier is 3 GHz, whereas it is 6 GHz at 60 GHz frequency. For each value of relative bandwidth, the two beams are represented here with 10000 equispaced continuous wave (CW) frequencies. In addition, various beam separations are used to examine interference from various angles. Initially, the beam of user 1 is at 0^o azimuth domain (boresight direction), whereas the beam of user 2 scans from $1^o - 10^o$ azimuth in 0.01^o steps. High observation and scanning precision were needed to demonstrate the effects of the squint in the extremely narrow spatial directions of the nulls in the provided simulation analysis. The presented method, on the other hand, does not require such precision because it uses the same beamformers for cancellations and useful beams, resulting in a cancellation null that moves in the same direction as the beam.

The mutual interference varies over the simulated beam separations. The interference from the beam of user 1 in the direction of user 2 is given in Fig. 8 for 3, 5 and 10% RBW. Similarly, squinting effects are more severe at scanning angles that have offset from the boresight direction. As a result, the direction of the interfering beam (ϕ_i) is also analyzed at a 15^o offset from the boresight, and beam of user 2 is scanned from $16^o - 25^o$ azimuth. User 1 IBI with offset from the boresight direction is also plotted in the Fig. 8 for 3, 5 and 10% RBW. To assess the results with and without offset from the boresight in the same figure, the inter-beam separation parameter is made relative the boresight direction. With the above definition, the scanning angles of the analysis results can be derived by simply adding the location of the interferer in the inter-beam separation.

When the IBI is examined from the direction of the nulls of the interfering beam in Fig. 8, it is seen that it increases with the

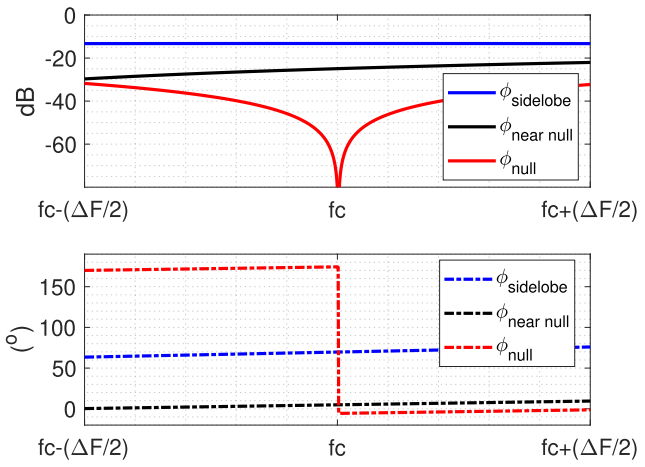

Fig. 9. The amplitude and phase response of wideband IBI channel with 5% relative bandwidth at first sidelobe maxima ($\phi_{sidelobe} = 5.135^o$), near null ($\phi_{nearnull} = 3.8^o$) and at first null ($\phi_{null} = 3.583^o$).

relative bandwidth. However, the IBI from the major lobes of the interfering beam decreases as the relative bandwidth increases. When the interfering beam is scanned away from the boresight, the squinting effect changes not only the levels, but also the spatial location of the lobes or nulls in the IBI. In other words, the expected interference from the null of the other beam may be caused by a squint-shifted lobe at higher relative bandwidth.

Wideband IBI behaves differently at the lobes than it does at the nulls or near nulls. Near null location of an interfering beam is interference from the direction which is between a sidelobe and a null. Fig. 9 illustrates the amplitude and phase response of the IBI with the relative bandwidth of 5% at the first sidelobe maxima, near null, and at the first null. The null depth in IBI for some frequencies around the carrier frequency can be observed to be quite deep. On the other hand, when the offset from the carrier frequency increases, the depth of the null decreases. The null channel appears to be the most frequency selective, followed by the near null and sidelobe channels. In comparison to the null, which fluctuates significantly over the wideband channel and has a shape similar to a spatial null, the amplitude response at sidelobe maxima changes little. At sidelobe maxima and near null, the phase response varies linearly over the wideband channel. For frequencies on either side of the symmetric band, the phase varies linearly in the direction of the first null, but it is different on both sides of the symmetric band.

B. Cancellation of Wideband IBI

The frequency selectivity of the wideband channel depends on the interference from the sidelobe, near null, or at the null position of the other beam. Therefore, the squinting effect is evaluated separately for the sidelobe, near null, and null of the interference-causing beam. In addition, the wideband squinting effect varies with the relative bandwidth and array size and is taken into account in this analysis.

In the analysis, a two-beam scenario serving two distinct users is simulated. Each beam is normalized to 0 dB. The beam of the first user is scanned to 15 degrees azimuth, and the beam of the second user is selected in the direction of the first sidelobe of the beam of the first user. Similarly, the location of beam 2 is changed to angular areas where it receives interference from beam 1 via its near null and null positions. The above angular configuration of the beams is used to categorize interference depending on frequency selectivity of the wideband channel of the IBI. Fig. 10(a)–(c) show the SINRs of beam 2 when beam 1 is interfering with its sidelobe, near null, and at null, respectively. Fig. 10(d)–(f) show the SINRs of beam 2 after canceling the interference from the sidelobe, near null, and null, respectively.

The maximum SINR value that user 2 can achieve is around 15 dBs, as shown in Fig. 10(a). Because the beam from the first user is causing interference with its first sidelobe, which has the relative power and therefore the SINR of the second user is limited by the relative power of the interfering sidelobe. Fig. 10(b) shows the SINR of user 2 when interference is coming from the near-null direction of the beam of user 1. When the relative bandwidth of the array increases, it is observed that the SINR decreases more for arrays with fewer than 64 antenna elements than for arrays with more than 64 antenna elements. This is because, in comparison to smaller arrays, the main and side lobes become narrower with larger arrays, and sidelobes spread in close proximity around the main lobe. Therefore, the squint shifted sidelobes away from the main lobe have lower power for larger arrays compared to smaller arrays.

Fig. 10(c) depicts the SINR of beam of user 2 with interference from the direction of the null of beam of user 1. In the direction of the null, there should be no power or very low power. As a result, interference from the direction of the null of the other beam should not degrade the SINR. When the array size is increased alone, the SINR has no noticeable effect. SINR is not much affected by the squinting effect for up to 3% of the relative bandwidth of the array. However, as the relative bandwidth of the array increases, the SINR drops more at smaller numbers of antennas than at larger numbers of antennas. This is because the squint shifted lobes that take the location of null in smaller arrays have a higher level than those in larger arrays.

When interference from the sidelobe of the beam 1 towards beam 2 given in Figs. 10(a) is cancelled with a single cross-coupling, the SINR of the beam 2 is shown in Fig. 10(d). The frequency of crosscoupling is set at the middle of the band. Good cancellation is accomplished because the sidelobes are less frequency selective than the near null and the null of an array. With the cancellation of the IBI, SINR of 40 dBs can be reached at smaller arrays. For example, 32 antenna elements with interference cancellation can achieve SINR of 40 dBs for 8% relative bandwidth of the arrays, 64 elements for roughly 5% relative bandwidth of the arrays, and so on. For larger arrays, the squint shifts the cancellation of the sidelobe to near null or null regions, which are more frequency selective.

Fig. 10(e) shows the SINR of user 2 after interference from the near null location of the other beam has been cancelled. User 2 achieves a SINR of roughly 40 dBs for any array size and up to 2% relative bandwidth. The near null are more frequency selective than the sidelobe regions. Squinting effects retain the interfering beam in the near null area for smaller arrays, which

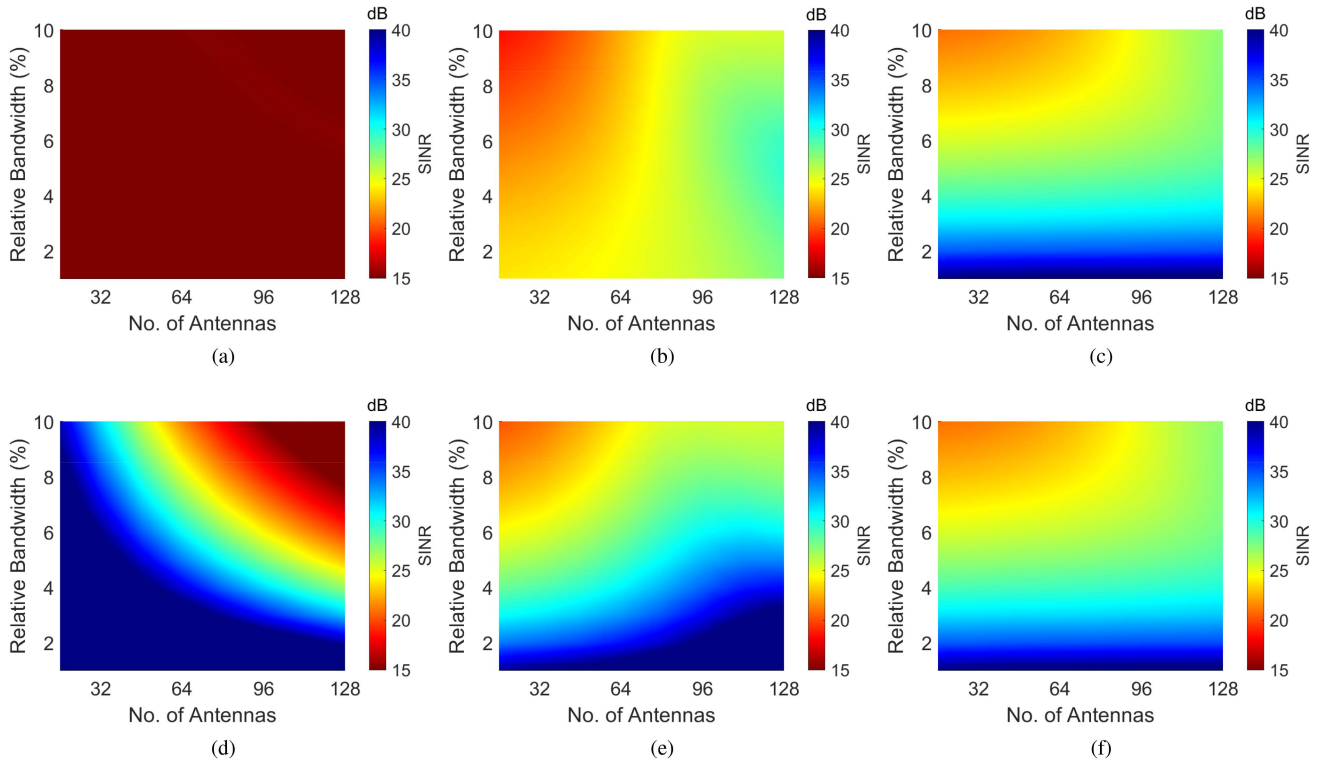

Fig. 10. SINR of the user 2 with inter-beam interference (IBI) from (a) sidelobe maxima, (b) near null, (c) null of the interfering beam, and with cancellation of IBI from (d) sidelobe maxima, (e) near null, (f) null, with the single crosscoupling (NXC=1) at the carrier frequency.

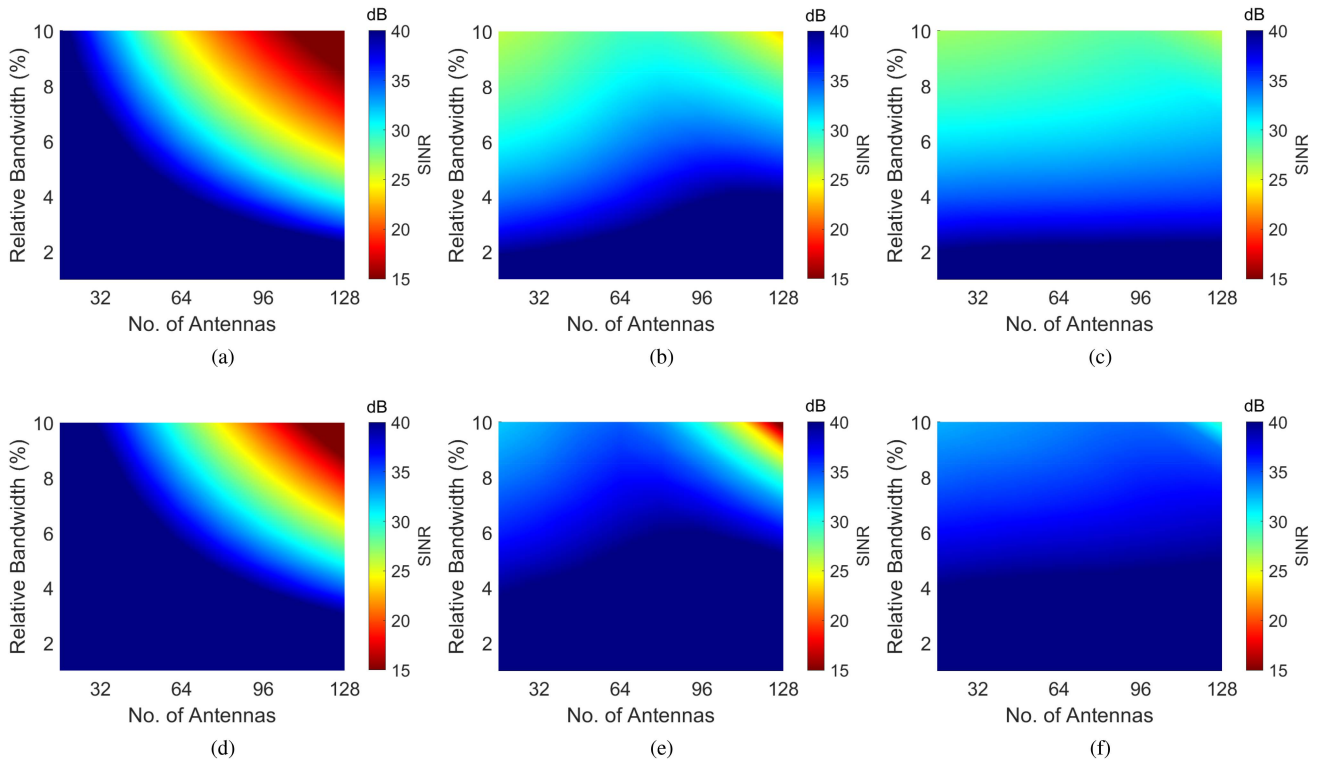

Fig. 11. SINR of the user 2 with inter-beam interference (IBI) cancellation at (a) sidelobe maxima, (b) near null, (c) null of the interfering beam with two crosscouplings (NXC=2), and with cancellation of IBI from (d) sidelobe maxima, (e) near null, (f) null, with the four crosscoupling (NXC=4).

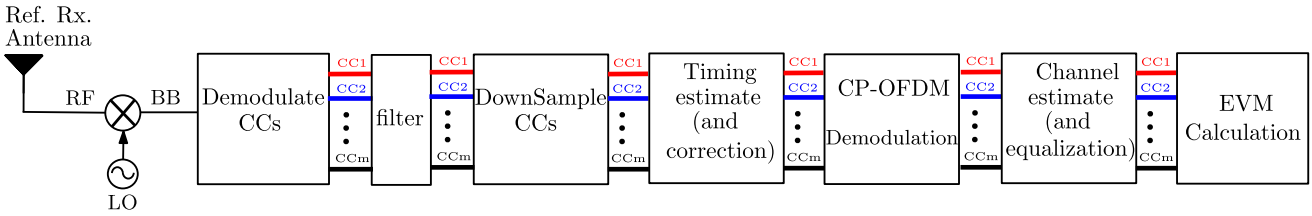

Fig. 12. Component carrier (CC) based wideband reference receiver.

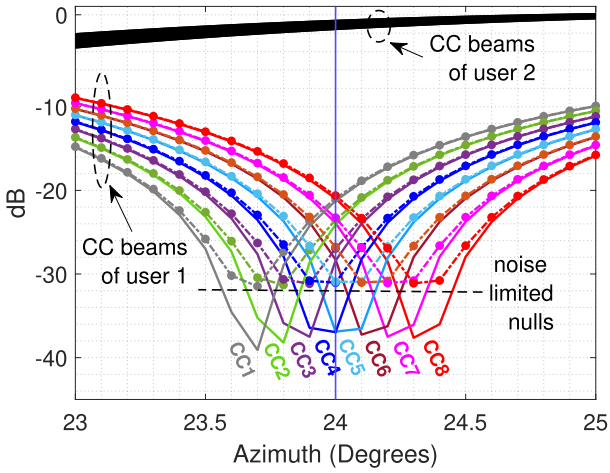

Fig. 13. Squinted nulls of the 8 CCs with single-cross-coupling (NXC = 1) and influence of the noise on the depth of the nulls.

reduces the interference cancellation performance and thus the SINR.

It is seen that the interference originating from the null of the beam is extremely frequency selective. Nulls are relatively narrow in angular space, therefore canceling them would necessitate more precision and accuracy in terms of phase and amplitude than canceling sidelobes or near nulls. Fig. 10(f) illustrates that after the IBI is cancelled from the null direction, there is no substantial impact on the improvement of the SINR. It is shown that there is no need for the IBI to be cancelled if the other beam is causing interference from the direction of the null and has a relative bandwidth of less than 3%. However, when the relative bandwidth of the array increases, a single crosscoupling is insufficient to improve the SINR with interference cancellation.

The approach presented in the paper divides the wideband channel into narrowband channels and conducts crosscoupling or cancellation independently on each narrowband channel for wideband interference cancellation. The absolute bandwidth is divided into N parts in the given analysis, with each part having its own crosscoupling to cancel interference. This method does not necessitate the modification of RF beamformers, implying that a single RF beamformer is utilized to enhance the wideband beamforming gain. Multiple crosscouplings are used to accomplish interference cancellation for the simulation analysis. Two and four crosscoupling are employed to cancel the interference in this case. The crosscoupling or cancellation frequency is set in the center of the band part for each crosscoupling. The cancellation of interference from the sidelobe, near null, and null with two crosscouplings is shown in Figs. 11(a)–(c). Figs. 11(d)–(f) depict the interference cancellation using four crosscouplings.

Multiple crosscoupling improves the cancellation of the interference in the presence of squinting effects, as expected. Furthermore, a larger relative bandwidth ratio is attained, canceling practically all interference with multiple crosscouplings. Multiple crosscouplings cancel interference all the way down to the noise floor, resulting in a higher relative bandwidth and better SINR range. Multiple crosscouplings have been observed to successfully cancel interference from sidelobe, near null, or null location of the interfering beam.

The analysis in this section showed that the squinting effect makes it harder for wideband phased arrays to cancel out interference. In addition, it is demonstrated that the performance of the cancellation changes based on the frequency selectivity of the interference channel, which in turn varies based on whether the interference originates from the sidelobe, near null, or null of the interfering beam. A single crosscoupling successfully eliminated sidelobe interference, but it is insufficient to handle the increased degree of frequency selectivity in the near null or null channel of the interference. Multiple crosscouplings, on the other hand, successfully canceled interference from the sidelobe, near null, or null channel of the interfering beam. For larger arrays and with a higher relative bandwidth, multiple crosscouplings also successfully eliminated interference between the beams of multiple users.

C. Cancellation of Wideband IBI With 5GNR Modulated Waveforms

In this subsection, an example case scenario of the two beams is simulated using standard 5GNR waveforms [35]. For each beam, a wideband waveform with eight CCs is used. Each CC is 100 MHz wide and separated from its neighbors by a 2.45 MHz guardband, as required by 3GPP NR standards. Two 16-element ULSAs are stacked on top of each other to serve two separate users in the spatial domain with user-specific data streams. At a carrier frequency of 27 GHz, inter-element spacing is kept to in the typical half-wavelength configuration for the ULA and also the eight CCs with guard bands aggregate to 822.32 MHz bandwidth, or relative bandwidth nearly equals to 3%.

The beam of user 1 is scanned at a 20^o azimuth angle, while the beam of user 2 is scanned at a 24^o azimuth angle with a 4^o angular separation. For 16-element ULSA, the half power beamwidth (HPBW) of the above arrangements is around 6.7^o. Consequently, the main lobes of the two beams interfere with each other in this example. With a single crosscoupling, the

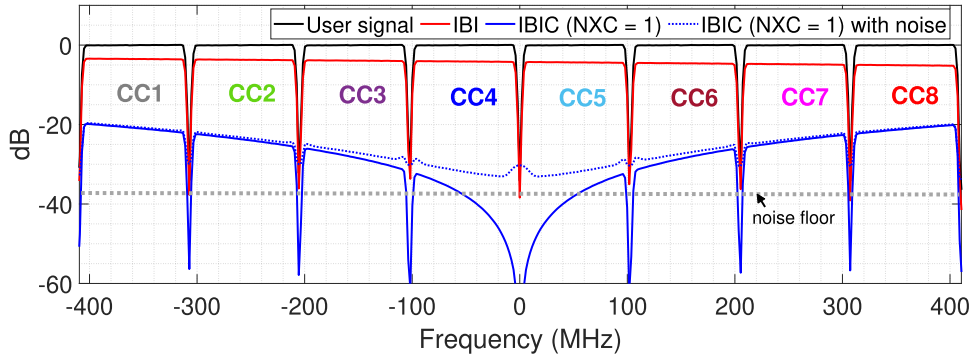

Fig. 14. Spectrum of the user signal, inter-beam interference (IBI), inter-beam interference cancellation (IBIC) with single crosscoupling (NXC=1), and the impact of noise on the performance of the cancellation.

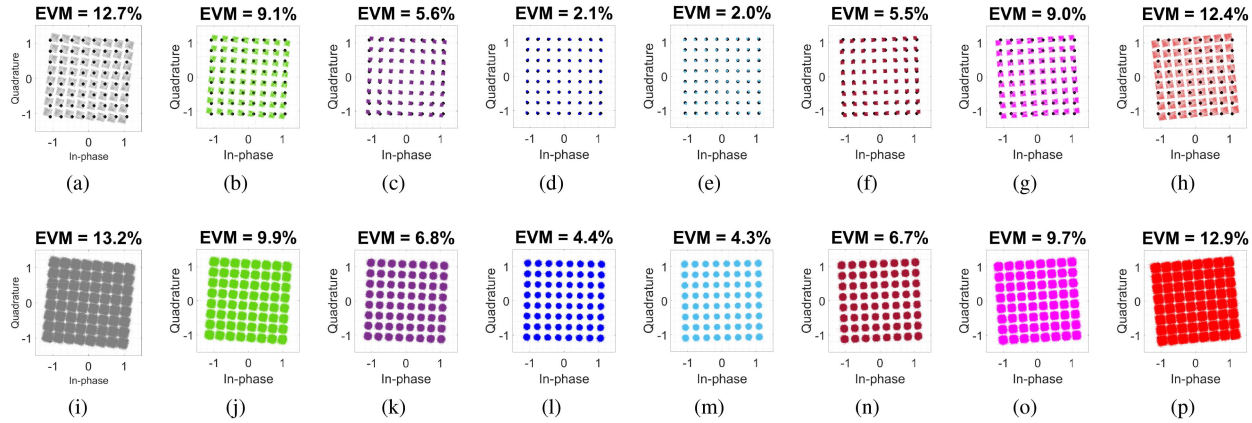

Fig. 15. Demodulated constellations of the CCs (1-8) with single crosscoupling (1XC) (a)-(h) without noise, and (i)-(p) with noise.

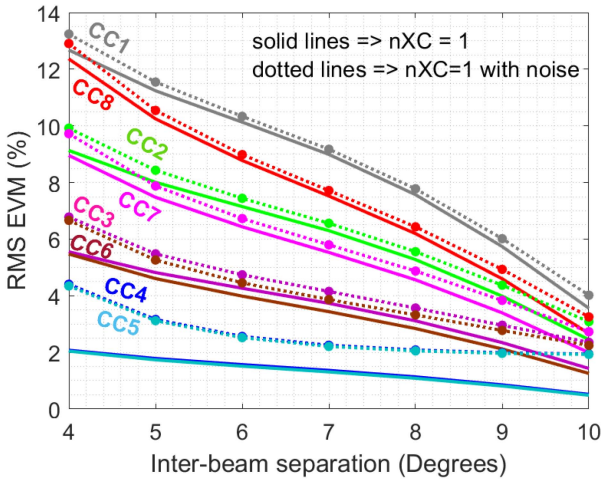

Fig. 16. EVM of 8 CCs with single crosscoupling at various inter-beam separation in the absence and presence of the noise (SNR = 35 dB).

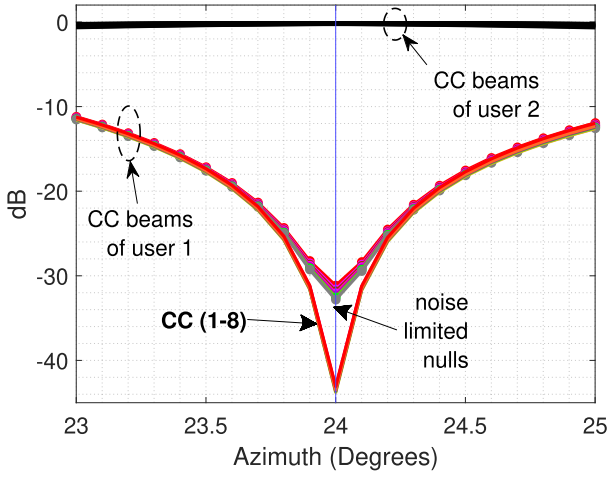

Fig. 17. Nulls of 8 CCs with eight cross-coupling (8XC) and influence of the noise on the depth of the nulls.

two beams are crosscoupled with each other, and the frequency of the crosscoupling is chosen to be the center frequency of the aggregated bandwidth. Spatial signals aimed at user 2 are received by a reference receiver antenna with a gain of 0 dB in the direction of user 2. A CC-based receiver is used to demodulate received signals, as shown in the Fig. 12. The receiver demodulates, filters, and downsamples each CC. Using downsampled CC signals, the timing is estimated and corrected. EVMs are determined using CP-OFDM demodulation after channel estimation and equalization.

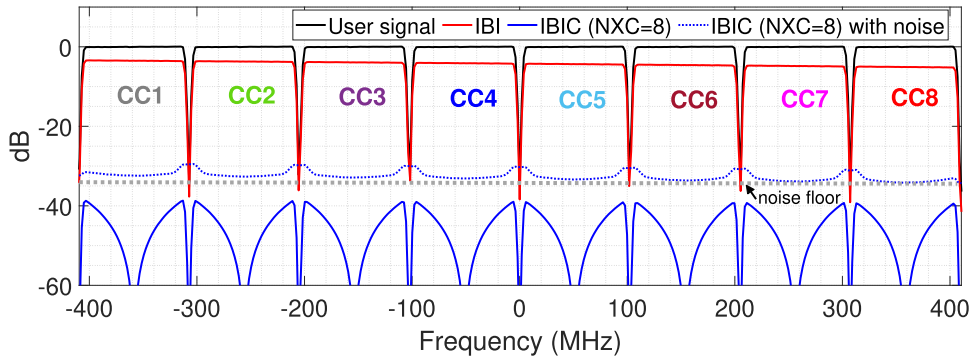

Fig. 18. Spectrum of the user signal, inter-beam interference (IBI), inter-beam interference cancellation (IBIC) with eight crosscouplings (NXC=8), and the impact of noise on the performance of the cancellation.

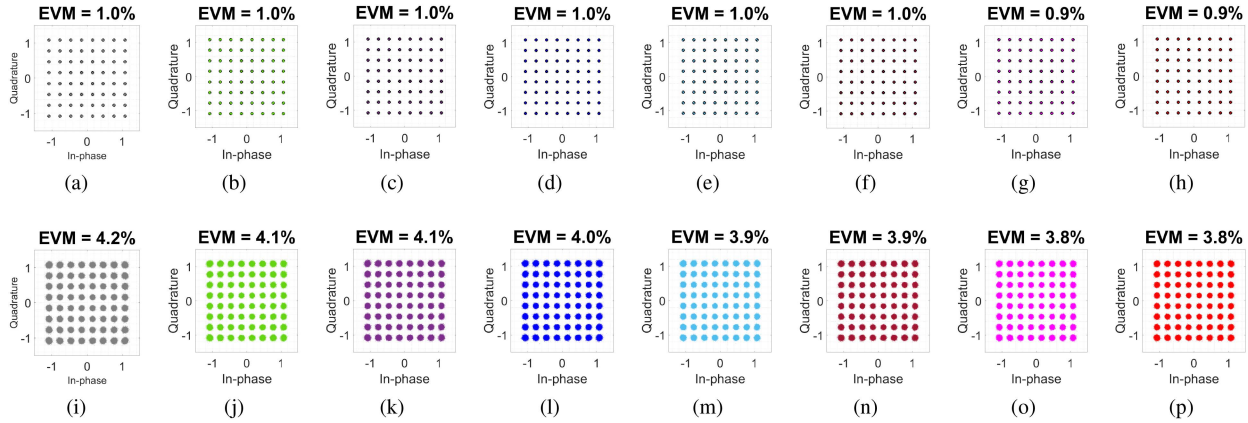

Fig. 19. Demodulated constellations of the CCs (1-8) with eight crosscoupling (8XC) (a)-(h) without noise, and (i)-(p) with noise (SNR=35 dB).

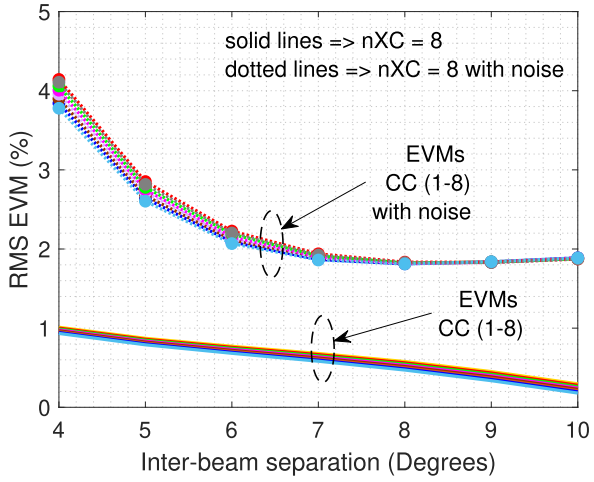

Fig. 20. EVM of 8 CCs with eight crosscouplings at various inter-beam separation in the absence and presence of the noise (SNR = 35 dB).

For wideband transmission, the beamformers should focus all CC beams towards the intended user, and each CC radiated pattern should have a null towards the interferer for interference cancellation. Due to the wideband squinting effect, the nulls of different CCs diverge from and limit their depths in the intended direction. In this example case scenario, we first examine at the formation of nulls in the spatial domain with a single crosscoupling. In the Fig. 13, spatial beams with 8 CCs from both users are simulated in the direction of user 2. The nulls of the various CCs of user 1 are not aligned in direction of user 2. Because CC1 has a higher offset from the center of the band than CC2, the null of the CC1 deviates more from the desired direction than the null of the CC2. Null formation for the other CCs is also examined. The null deviation of a CC is determined by its offset from the crosscoupling frequency. When a null deviates from its intended direction, its null depth decreases in that direction, resulting in increased interference. Furthermore, in the presence of noise, the nulls of various CCs are confined to the noise floor, which is 35 dB lower than the signal power in this example.

Fig. 14 shows the spectrums of the user signal, inter-beam interference (IBI), and cancelled IBI with crosscouplings for frequency domain analysis. The analysis also includes the spectrum of the cancelled IBI in the presence of noise. As seen in the spectrum, the level of IBI is approximately 4 dB less than the signal power without interference cancellation or crosscoupling. When IBI is cancelled with a single crosscoupling, a deep null is seen in the cancelled spectrum of IBI at the frequency of the crosscoupling. However, as the frequency offset from the crosscoupling frequency increases, the depth of the null decreases due to the squint effect. As a result, the degree

of squinting differs between CCs. Compared to CCs that are closer to the crosscoupling frequency, those that are farther away exhibit more squint. IBI cancellation with crosscoupling is essentially constrained by the squinting effect in the absence of noise. The noise floor, on the other hand, limits the deep null of the crosscoupling frequency in the presence of noise.

Additionally, we examine the effects of squint and noise on the received signal constellations. CC constellations from 1 to 8 of user 2 with a single crosscoupling are shown in the Fig. 15(a)–(h). The CC with a greater degree of squint have a greater degree of rotation in their constellations. The size of the error vector varies with the amount of interference in the constellation, while the phase rotation of the error vector is affected by the squint of the interfering signal. In the presence of noise, no more rotations of the constellation are detected; nonetheless, the noise increases the amplitude of the error vector, as shown in Fig. 15(i)–(p).

Furthermore in this simulation analysis, interference cancellation is also examined with a single cross-coupling at various inter-beam separations. The beam of user 1 remains at a 20^o azimuth, but the beam of user moves in one-degree steps from a 24^o azimuth to a 30^o azimuth. All 8 CCs are demodulated for user 2 for each inter-beam separation selection, and EVMs are shown in the Fig. 16. As beam separation increases, the EVMs of all CCs fall, but the degree varies depending on the squinting effect in each CC. The noise has an impact on the EVMs as well. The EVMs of those CCs with less squint appear to be mainly degraded by noise.

The performance of wideband interference cancellation is also examined using multiple crosscouplings. Therefore, eight crosscouplings are used for the eight CCs, one for each CC. For each CC, the crosscoupling frequency is selected at the middle of each CC. Fig. 17 shows the spatial beams of both users, with 8 CCs simulated in the direction of user 2. The nulls of different CC of user 1 are aligned in the direction of user 2. The noise-limited nulls are also aligned in the desired direction.

The frequency domain performance of multiple crosscoupling is also addressed. Fig. 18 shows the spectrums of the signal of user 2, IBI towards user 2, and cancelled IBI with eight crosscouplings. The spectrum of the cancelled IBI under noise influence is also included. When IBI is cancelled by a separate crosscoupling for each CC, the interference in the center of each CC exhibits a deep null. The use of eight crosscouplings reduces interference over the wide bandwidth. The spectrum of the IBI with eight crosscouplings is much lower than the user signal in the absence of noise. The cancelled spectrum of IBI is confined to the noise floor in the presence of noise.

Squint has an effect on the constellations of received CC signals as well. Fig. 19(a)–(h) depict the constellations of the CCs from 1 to 8 of user 2 with eight crosscoupling cancellers. Because a separate crosscoupling effectively cancels the interference in each CC, the demodulated constellations of the CCs have no rotation. Therefore, the magnitude of the error vector increases with noise as shown in the Fig. 19(i)–(p).

In the simulation analysis, the interference cancellation by eight cross-couplings is also analyzed at various inter-beam separations. The beam of user 1 is fixed at a 20^o azimuth, and the beam of user moves in one-degree steps from 24^o to 30^o azimuth. For each separation of the beams, 8 CCs are demodulated for the user 2, and EVMs are displayed in Fig. 20. It is seen that when beam separation increases, the EVMs of all the 8 CCs stay less than 1%, and the magnitude of the EVMs remains consistent across all CCs. Furthermore, when interference is completely cancelled, the noise has a same effect on the EVMs of all the CCs.

IV. Conclusion

The cancellation of wideband inter-beam interference is highly frequency selective. It has different behaviour at major lobes, near nulls, and nulls. The wideband squinting effect reduces spatial selectivity in transmission, lowering null depth towards other beams and lowering the achievable SINR of the multibeam system. The wideband squinting effect is further affected by the relative bandwidth of the array, scanning angles of the main lobe and IBI cancellations, and the number of antennas, which are considered in the paper. This paper presents and analyses a two-stage beamforming technique for enhancing the SINR of multibeam systems. Crosscoupled cancellation paths are used to minimize interference in one stage, while beamformers are employed to improve the EIRP of the beams in the subarrays. A component carrier-based crosscoupling technique is described for the cancellation of the wideband IBI. This method nicely channelizes signals in the frequency domain, and this enables a separate crosscoupling for each CC in order to achieve wideband cancellation of the IBI. Simulation analysis shows that the squinting effect makes it difficult for wideband phased arrays to cancel interference. It also shows that cancellation performance depends on the frequency selectivity of the interference channel, which varies depending on whether the interference comes from the sidelobe, near null, or null of the interfering beam. A single crosscoupling eliminates sidelobe interference but is insufficient to manage the enhanced frequency selectivity in the near null or null interference scenario. The sidelobe, near null, or null channel of the interfering beam can be eliminated by multiple crosscouplings. For larger arrays with a wider relative bandwidth, multiple crosscouplings can cancel out the interference between the beams of different users. The analysis in the paper gives insights into how relative bandwidth can be taken into account when mmW signals are channelized in the frequency domain enabling relatively simple and effective means for inter-beam interference cancellation in multibeam transmissions. Such information could be utilized for example when designing next-generation waveforms and signal structures for 6 G communications and sensing. The analysis derived in this paper assumed LOS propagation conditions which are typical in mmW systems. In case of multiple propagation paths appearing in the directions of the narrow main beams, the frequency selectivity of the channels may require to divide the signals into much smaller bands that can be then individually cancelled, similarly as in case of LOS channel with beam squint.

References

[1] T. S. Rappaport, Y. Xing, G. R. MacCartney, A. F. Molisch, E. Mellios, and J. Zhang, "Overview of millimeter wave communications for fifth-generation (5G) wireless networks—with a focus on propagation models," *IEEE Trans. Antennas Propag.*, vol. 65, no. 12, pp. 6213–6230, Dec. 2017.

[2] A. S. Cacciapuoti, K. Sankhe, M. Caleffi, and K. R. Chowdhury, "Beyond 5G: THz-based medium access protocol for mobile heterogeneous networks," *IEEE Commun. Mag.*, vol. 56, no. 6, pp. 110–115, Jun. 2018.
[3] M. A. Uusitalo et al., "6G vision, value, use cases and technologies from European 6G flagship project Hexa-X," *IEEE Access*, vol. 9, pp. 160004–160020, 2021.
[4] K. Guan et al., "On millimeter wave and THz mobile radio channel for smart rail mobility," *IEEE Trans. Veh. Technol.*, vol. 66, no. 7, pp. 5658–5674, Jul. 2017.
[5] T. S. Rappaport et al., "Wireless communications and applications above 100 GHz: Opportunities and challenges for 6G and beyond," *IEEE Access*, vol. 7, pp. 78729–78757, 2019.
[6] S. Sun, T. S. Rappaport, M. Shafi, P. Tang, J. Zhang, and P. J. Smith, "Propagation models and performance evaluation for 5G millimeter-wave bands," *IEEE Trans. Veh. Technol.*, vol. 67, no. 9, pp. 8422–8439, Sep. 2018.
[7] R. W. Heath, N. Gonzz-Prelcic, S. Rangan, W. Roh, and A. M. Sayeed, "An overview of signal processing techniques for millimeter wave MIMO systems," *IEEE J. Sel. Topics Signal Process.*, vol. 10, no. 3, pp. 436–453, Apr. 2016.
[8] T. Tuovinen, N. Tervo, and A. Pärssinen, "Analyzing 5G RF system performance and relation to link budget for directive MIMO," *IEEE Trans. Antennas Propag.*, vol. 65, no. 12, pp. 6636–6645, Dec. 2017.
[9] K. Rikkinen, P. Kyosti, M. E. Leinonen, M. Berg, and A. Parssinen, "THz radio communication: Link budget analysis toward 6G," *IEEE Commun. Mag.*, vol. 58, no. 11, pp. 22–27, Nov. 2020.
[10] J. G. Andrews, T. Bai, M. N. Kulkarni, A. Alkhateeb, A. K. Gupta, and R. W. Heath, "Modeling and analyzing millimeter wave cellular systems," *IEEE Trans. Commun.*, vol. 65, no. 1, pp. 403–430, Jan. 2017.
[11] S. Han, C.-l. I., Z. Xu, and C. Rowell, "Large-scale antenna systems with hybrid analog and digital beamforming for millimeter wave 5G," *IEEE Commun. Mag.*, vol. 53, no. 1, pp. 186–194, Jan. 2015.
[12] J. A. Zhang, X. Huang, V. Dyadyuk, and Y. J. Guo, "Massive hybrid antenna array for millimeter-wave cellular communications," *IEEE Wireless Commun.*, vol. 22, no. 1, pp. 79–87, Feb. 2015.
[13] P. Kyösti, M. F. De Guzman, K. Haneda, N. Tervo, and A. Psinen, "How many beams does Sub-THz channel support," *IEEE Antennas Wireless Propag. Lett.*, vol. 21, no. 1, pp. 74–78, Jan. 2022.
[14] O. E. Ayach, S. Rajagopal, S. Abu-Surra, Z. Pi, and R. W. Heath, "Spatially sparse precoding in millimeter wave MIMO systems," *IEEE Trans. Wireless Commun.*, vol. 13, no. 3, pp. 1499–1513, Mar. 2014.
[15] C. A. Balanis, *Antenna Theory: Analysis and Design*, 4th ed. Hoboken, NJ, USA:Wiley, 2015.
[16] J.-C. Chen, "Hybrid beamforming with discrete phase shifters for millimeter-wave massive MIMO systems," *IEEE Trans. Veh. Technol.*, vol. 66, no. 8, pp. 7604–7608, Aug. 2017.
[17] X. Gao, L. Dai, and A. M. Sayeed, "Low RF-Complexity technologies to enable millimeter-wave MIMO with large antenna array for 5G wireless communications," *IEEE Commun. Mag.*, vol. 56, no. 4, pp. 211–217, Apr. 2018.
[18] M. Jokinen, O. Kursu, N. Tervo, J. Saloranta, M. E. Leinonen, and A. Psinen, "Over-the-air phase measurement and calibration method for 5G mmW phased array radio transceiver," in *Proc. ARFTG Microw. Meas. Conf.*, 2019, pp. 1–4.
[19] B. Wang, F. Gao, S. Jin, H. Lin, and G. Y. Li, "Spatial- and frequency-wideband effects in millimeter-wave massive MIMO systems," *IEEE Trans. Signal Process.*, vol. 66, no. 13, pp. 3393–3406, Jul. 2018.
[20] S. Noh, J. Lee, H. Yu, and J. Song, "Design of channel estimation for hybrid beamforming millimeter-wave systems in the presence of beam squint," *IEEE Syst. J.*, vol. 16, no. 2, pp. 2834–2843, Jun. 2022.
[21] Q. Wan, J. Fang, Z. Chen, and H. Li, "Hybrid precoding and combining for millimeter Wave/Sub-THz MIMO-OFDM systems with beam squint effects," *IEEE Trans. Veh. Technol.*, vol. 70, no. 8, pp. 8314–8319, Aug. 2021.
[22] M. Y. Javed, N. Tervo, M. E. Leinonen, and A. Psinen, "Spatial interference reduction by subarray stacking in large two-dimensional antenna arrays," *IEEE Trans. Antennas Propag.*, vol. 69, no. 7, pp. 3863–3874, Jul. 2021.
[23] S. Applebaum, "Adaptive arrays," *IEEE Trans. Antennas Propag.*, vol. 24, no. 5, pp. 585–598, Sep. 1976.
[24] H. Steyskal, R. Shore, and R. Haupt, "Methods for null control and their effects on the radiation pattern," *IEEE Trans. Antennas Propag.*, vol. 34, no. 3, pp. 404–409, Mar. 1986.
[25] R. Haupt, "Phase-only adaptive nulling with a genetic algorithm," *IEEE Trans. Antennas Propag.*, vol. 45, no. 6, pp. 1009–1015, Jun. 1997.
[26] A. F. Morabito and P. Rocca, "Optimal synthesis of sum and difference patterns with arbitrary sidelobes subject to common excitations constraints," *IEEE Antennas Wireless Propag. Lett.*, vol. 9, pp. 623–626, 2010.
[27] S. W. Peters and R. W. Heath, "Cooperative algorithms for MIMO interference channels," *IEEE Trans. Veh. Technol.*, vol. 60, no. 1, pp. 206–218, Jan. 2011.
[28] N. Tervo, J. Aikio, T. Tuovinen, T. Rahkonen, and A. Parssinen, "Digital predistortion of amplitude varying phased array utilising over-the-air combining," in *Proc. IEEE MTT-S Int. Microw. Symp.*, 2017, pp. 1165–1168.
[29] N. Tervo et al., "Combined sidelobe reduction and omnidirectional linearization of phased array by using tapered power amplifier biasing and digital predistortion," *IEEE Trans. Microw. Theory Techn.*, vol. 69, no. 9, pp. 4284–4299, Sep. 2021.
[30] R.V. Gatti, M. Dionigi, and R. Sorrentino, "Computation of gain, noise figure, and third-order intercept of active array antennas," *IEEE Trans. Antennas Propag.*, vol. 52, no. 11, pp. 3139–3143, Nov. 2004.
[31] P. G. Vouras and T. D. Tran, "Robust transmit nulling in wideband arrays," *IEEE Trans. Signal Process.*, vol. 62, no. 14, pp. 3706–3719, Jul. 2014.
[32] S. K. Garakoui, E. A. M. Klumperink, B. Nauta, and F. F. E. Van Vliet, "A 1-to-2.5 GHz phased-array IC based on gm-RC all-pass time-delay cells," in *Proc. IEEE Int. Solid-State Circuits Conf.*, 2012, pp. 80–82.
[33] L. Zhang, A. Natarajan, and H. Krishnaswamy, "Scalable spatial notch suppression in spatio-spectral-filtering MIMO receiver arrays for digital beamforming," *IEEE J. Solid-State Circuits*, vol. 51, no. 12, pp. 3152–3166, Dec. 2016.
[34] R. J. Mailloux, *Phased Array Antenna Handbook*, 2nd ed.Norwood, MA, USA: Artech House, 2018.
[35] 3rd Generation Partnership Project (3GPP), "Technical specification group radio access network; NR; base station (BS) radio transmission and reception," 3GPP, Sophia Antipolis, France, Tech. Specification 38.104, Sep. 2021.
[36] R. Akbar et al., "A wideband IF receiver module for flexibly scalable mmWave beamforming combining and interference cancellation," in *Proc. IEEE Eur. Solid State Circuits Conf.*, 2019, pp. 213–216.

Muhammad Yasir Javed (Graduate Student Member, IEEE) received the B.Eng. degree in telecommunication from the National University of Modern Languages, Islamabad, Pakistan, in 2013, and the M.Sc. degree in wireless communication engineering in 2017 from the University of Oulu, Oulu, Finland, where he is currently working toward the Ph.D. degree with the Centre for Wireless Communications. His research interests include millimeter-wave, phased array, multibeam RF architectures, and interference reduction techniques.

Nuutti Tervo (Member, IEEE) received the B.Sc. (Tech.), M.Sc. (Tech.), and D.Sc. (Tech.) degrees (with distinctions) from the University of Oulu, Oulu, Finland, in 2014 and 2022, respectively. His doctoral dissertation research focused on nonlinearity and linearization of millimeter-wave beamforming transceivers. Since 2022, he has been a Postdoctoral Researcher with the Centre for Wireless Communications – Radio Technologies (CWC-RT) Research Unit, University of Oulu. He has a strong background in different fields of wireless communications, including radio frequency, radio channel modeling, signal processing, and system-level analysis. Around those topics, he has already authored or coauthored more than 60 international journal and conference papers and he holds patents. In 2019, he was the recipient of the Young Scientist Award of the URSI XXXV Finnish Convention on Radio Science, Tampere, and in 2020, he coauthored the paper that was the recipient of the 50th EuMC Microwave Prize 2020, Utrecht, Netherlands.

Marko E. Leinonen (Member, IEEE) received the M.Sc., Licentiate in Technology and Doctor of Science degrees in electrical engineering from the University of Oulu, Oulu, Finland, in 1996, 2002 and 2020, respectively. From 1994 to 2012, he was with Nokia Mobile Phones, Oulu, working with various positions with radio engineering and technology management. From 2006 to 2007, he was a Senior Engineering Manager in Bangalore, India. From 2012 to 2016, he was a Master Developer with Ericsson, Oulu. Since 2017, he has been with the Centre for Wireless Communications, University of Oulu, where he is currently a Research Director. He holds more than 40 granted international patent families concentrating on radio engineering. His research interests include wireless radio systems and quality topics in radio engineering.

Aarno Pärssinen (Senior Member, IEEE) received the M.Sc., Licentiate in Technology and Doctor of Science degrees in electrical engineering from the Helsinki University of Technology, Helsinki, Finland, in 1995, 1997 and 2000, respectively. From 1994 to 2000, he was with Electronic Circuit Design Laboratory, Helsinki University of Technology, Finland, working on direct conversion receivers and subsampling mixers for wireless communications. In 1996, he was a Research Visitor with the University of California at Santa Barbara, Santa Barbara, CA, USA. From 2000 to 2011, he was with Nokia Research Center, Helsinki, Finland. During 2009–2011, he was a Member of Nokia CEO Technology Council. From 2011 to 2013, he was a Distinguished Researcher and RF Research Manager with Renesas Mobile Corporation, Helsinki. From October 2013 to September 2014, he was an Associate Technical Director with Broadcom, Helsinki. Since September 2014, he has been with the Centre for Wireless Communications, University of Oulu, Oulu, Finland, where he is currently a Professor. He leads Devices and Circuits research area in 6G Flagship Program financed by Academy of Finland. He has authored and coauthored one book, two book chapters, more than 200 international journal and conference papers and holds several patents. His research interests include wireless systems and transceiver architectures for wireless communications with special emphasis on the RF and analog integrated circuit and system design. He is also one of the original contributors to Bluetooth low energy extension, now called as BT LE. He was a Member of the technical program committee of International Solid-State Circuits Conference during 2007–2017, where he was the Chair of European regional committee during 2012–2013, and Chair of the wireless sub-committee during 2014–2017. He was Solid-State Circuits Society representative for IEEE 5G initiative during 2015–2019. He was the recipient of European Microwave Price on the best paper of the European Microwave conference 2020.